# Thermal annealing effects on the structural and electrical properties of $Ag_2La$ thin films deposited by thermal evaporation technique

A. F. Qasrawi[a,b,*], W. A. Zakarneh[a]
[a]*Department of Physics, Arab American University, Jenin, Palestine*
[b]*Department of Electrical and Electronics Engineering, Istinye University, 34010, Istanbul, Turkey*

Herein $Ag_2La$ thin films are fabricated by a vacuum coating method and subjected to a thermal annealing process. The thermally heated of films at 200 $^oC$ increased the crystallite sizes and improved the crystalline structure of the films. For these films the electrical conductivity measurements which were handled in the temperature range of 300-440 K. The conductivity analyses indicated that the transport of charged particles is dominated by the thermionic emission and by the variable range hopping conduction mechanisms. The annealing of films shifted the impurity levels and decreased; the degree of disorder, the average hopping distance and the average hopping energy.

(Received April 7, 2024; Accepted June 17, 2024)

*Keywords:* $Ag_2La$, Orthorhombic, Annealing, Conductivity, Variable range hopping

## 1. Introduction

Thin film alloys have recently attracted attention due to their wide range of applications across various fields of technology. They can be used as promising coatings suiting electro-mechanical systems [1], optoelectronic devices [2] and memory devices [3] as well. They contribute to enhancing the performance of numerous electronic devices. As for examples copper nanowires and silver nanosheets were used in the fabrication of bimetallic nanocomposites [4]. These silver rich nanocomposites showed high sensitivity up to $2.033\times 10^{-3}$ $A/mM^1cm^2$ and a fast amperometric response. These features make them hold promise for fabrication of flexible electrochemical devices [4]. In addition silver layers formed from silver nanoparticles were found ideal for power device applications [5]. These layers exhibited long life workability exceeding 1000 hours even at high temperature of 250 $^oC$ [5]. Thin film alloys are also used in the fabrication of micro-switches, sensors, and magnetic read heads [6].

We were motivated by the simplicity of fabrication and the broad application potential of these alloys to create a new class of alloy thin films incorporating silver and lanthanum metals. Silver based alloys is known for their thermal stability [2]. Lanthanum is also a highly reactive material and forms alloys easily [7]. $LaGe_2$ thin films are found suitable as band filters exhibiting cutoff frequency of 200 GHz. The films were ideal for use in 6G technology [7]. The novelty of the current work is that new class of alloys are formed by coating layers of Ag onto layers of La. The layered structures, fabricated via thermal evaporation under a vacuum pressure of $10^{-5}$ mbar, demonstrate unique physical characteristics distinct from individual Ag or La films. The simplicity of forming $Ag_2La$ alloys which are actualized by stacking the individual Ag and La layers is regarded as a novel easy way to produce thin film alloys. The research will investigate the crystal structure, surface analyses including morphology, atomic contents, and electrical characteristics of the alloys. Computational software will aid in structural analysis and bond distance visualization. Annealing at 200°C in air will be performed to observe its effects on structural and electrical properties. Emphasis will be placed on understanding the current conduction mechanism, including thermionic and variable range hopping parameters such as impurity levels, disorder degree, hopping distances and energies, and localized density of states near the Fermi level.

* Corresponding author: atef.qasrawi@aaup.edu
https://doi.org/10.15251/DJNB.2024.192.909

## 2. Experimental details

$Ag_2La$ thin films were accidentally produced during the coating of stacked layers of lanthanum and silver nanosheets. Each of these two nanosheets was 100 nm thick. They undergo coating via the thermal evaporation method in a vacuum environment with a pressure of $10^{-5}$ mbar, employing the NORM-VCM-600 thermal evaporator. The deposition of the films was initiated by inserting high purity (99.99%) lanthanum powders purchased from Alpha Aeser firm into the evaporator and coating it onto glass substrates cleaned using ultrasonic vibration machine. The produced glass/La layers were then employed as substrates to coat another 100 nm thick layer of Ag. Pure silver nanopowders ordered from Alpha Aeser firm were used as evaporation sources. Some of the produced films were heated at 200 $^oC$ in air for one hour. The produced glass/La/Ag films were then studied with the help of a Miniflex 600-XRD unit working at scanning speed of 0.5 deg./min to explore the structure. The morphology and compositional analyses were handled with the help of a scanning electron microscope (COXEM-200). The microscope have an EDAX type analyzer to identify the X-ray energy dispersion. The electrical studies were actualized on a Hall bar shaped films. Electrical contacts to the Hall bar films were made from gold films. The conductivity response to temperature variations was investigated using a specialized cryostat setup. This equipment integrates an automated Keithley current-voltage system featuring a 6485 picoammeter and Keithley 230 programmable voltage source. Measurements were conducted within the temperature range of 300-440 K. The conductivity type of the films was determined using the hot probe technique, revealing n-type conductivity.

## 3. Results and discussion

The X-ray diffraction (XRD) findings for dual stacked layers comprising lanthanum and silver, each with a thickness of 100 nm, are illustrated in Figure 1(a).The XRD patterns for these layers revealed diffraction peaks centered at diffraction angles different from those of cubic Ag (Joint Committee on Powder Diffraction Standard: JCPDS, file No. 04-0783), hexagonal La, cubic $Ag_2O$ ((JCPDS: 89-3722)) and $La_2O_3$ (JCPDS: 05-0602). The observed XRD patterns are analyzed using "TREOR 92" and "Crystdiff" software packages. The diffraction patterns displayed in Fig .1 (a) are best fitted with the orthorhombic structure of $Ag_2La$. However the low dimensional $Ag_2La$ films exhibit different lattice parameters from those reported for orthogonal $Ag_2La$ bulky samples. For the currently reported thin films the lattice constants of the orthorhombic cell are $a = 6.670$ Å$, b = 10.386$ Å$, c = 7.749$ Å corresponding to a space group number71 ($Immm$). Those reported in literature displayed values of $a = 4.825$ Å$, b = 7.287$ Å$, c = 8.196$ Å and space group number 74 ($Imma$) for $Ag_2La$ bulks obtained by the melting technique [8]. The lattice constants change due to the more lattice strain associated with the low dimension of the grown films [9]. To gain knowledge about the bond lengths of the low dimensional orthorhombic $Ag_2La$ cells we have rebuilt the crystal using "Crystal Maker" software packages. The schematics of the $Ag_2La$ crystals are shown in Fig. 2 (b). A shortest bond distance of 1.35 Å is measured for Ag1-La bond. The second bond Ag atom Ag2-La exhibited lattice distance of 2.296 Å. Ag1-Ag2 bonds exhibit length of 1.68 Å. The formed $Ag_2La$ films show bond lengths lower than those of La-La (382 pm [10]) and Ag-Ag (253 pm [11]). When coating Ag films onto La, the shorter bond length of Ag1-La and Ag2-La make the formation of $Ag_2La$ preferable to reach thermodynamic stability [12], [13]. More stable bonds leads to stronger electron dissociation on the atom. The latter manifest itself in the broadening of the bandwidth and increase in the density of states [14]. On the other hand, the calculated structural parameters including the crystallite size ($D = \frac{0.94\,\lambda}{\beta\, cos\theta}$ [8]; $\beta$: maximum peak broadening), the strain ($\varepsilon = \frac{\beta}{4\, tan\theta}$ [8]), the stacking faults percentages ($SF\%=100.\frac{2\pi^2\beta}{45\sqrt{3\tan(\theta)}}$ [8]) and defect density ($\delta_a = 15 \in/(aD)$ along the $a-$axis [8]) are show in Table-1. The parameters are consistent with Ag based materials like $Ag_2O$ where crystallite sizes and defect densities of 27 nm and $1.4\times 10^{11}$ $cm^{-2}$ are reported [15].

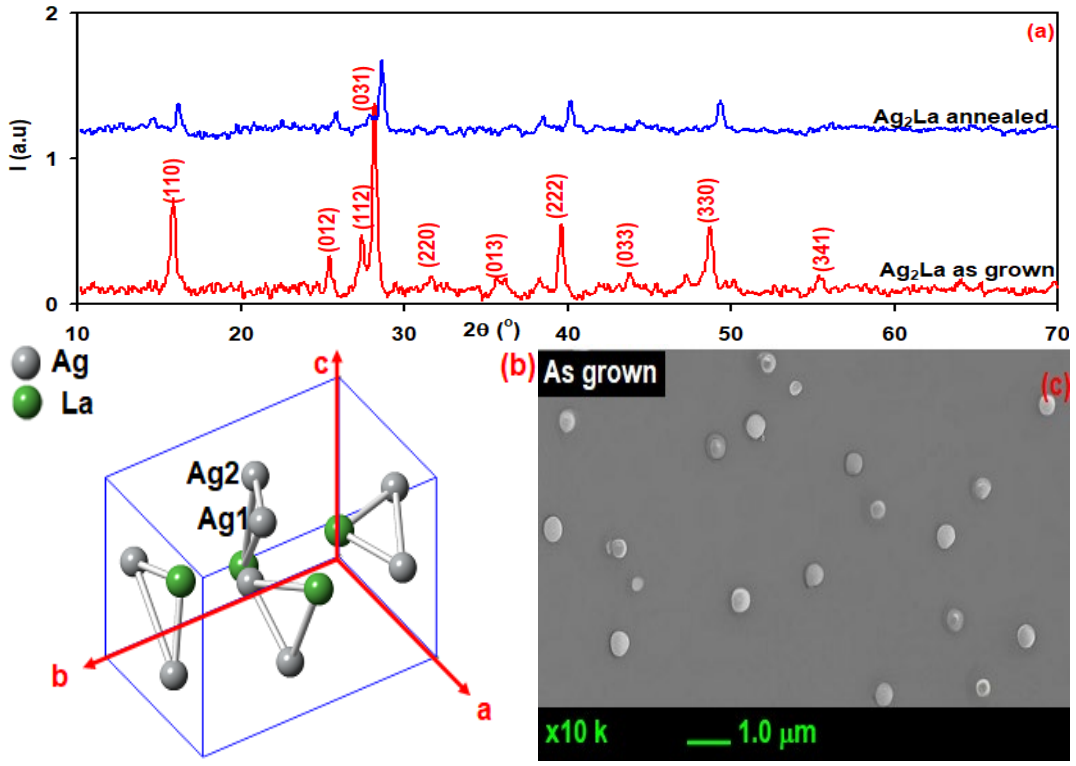


*Fig. 1. (a) The XRD graphs for the as deposited and annealed $Ag_2La$ films. (b) Showing the schematic for the crystalline phase and (c) show the SEM images for the as grown $Ag_2La$ samples.*

Fig. 1 (c) show the SEM images for the as deposited $Ag_2La$ films. The films contained irregular distribution of spherical grains. The average sizes of the grains is 400 nm. In addition the EDS spectra for $Ag_2La$ samples are illustrated in Fig. 2. The figure indicates the existence of O, Si, Na. Mg, Ca, Au, Ag and La metals only. The Si, O, Na, Mg and Ca elements are related to the glass slides used as substrates ($SiO:Na_2O:MgO:CaO$). The goild is present because the samples were covered with few nanometers of gold to avoid electron contaminations during SEM and EDS recording. The atomic contents of Ag and La in the films were found to be of 68.25 at. % Ag and 31.75 at. La. The chemical formula for this alloy is $Ag_{2.15}La$. Some excess Ag existed in the samples. Excess Ag is a main reason for the n-type behavior of the films.

*Table 1. The mechanical parameters for the as grown and annealed $Ag_2La$ films.*

| sample | $2\theta(^o)$ | D (nm) | $\varepsilon x10^{-3}$ | SF% | a (Å) | b (Å) | c (Å) | $\delta(x10^{11}$ line/cm$^2$) |
|---|---|---|---|---|---|---|---|---|
| As grown | 28.1 | 29 | 5.14 | 0.26 | 6.670 | 10.386 | 7.485 | 3.99 |
| Annealed | 28.6 | 34 | 4.28 | 0.22 | 6.431 | 10.215 | 7.473 | 2.91 |

On the other hand the effect of thermal annealing at 200 $^oC$ in the air atmosphere on the $Ag_2La$ films is studied. As can be seen from Fig.1 (a) the peaks are shifted toward larger diffraction angles indicating the shrinkage in the unit cell parameters. The re-calculated lattice parameters showed values of $a = 6.431$ Å, $b = 10.215$ Å, $c = 7.473$ Å. Simulation of the new resulting crystals displayed bond distances of 1.34 Å, 2.076 Å and 1.376 Å, for Ag1-La, Ag2-La and Ag1-Ag2, bonds respectively. The bond lengths are also decreased indicating stronger bonding in the annealed films as compared to the as grown which displayed respective bond lengths of 1.35 Å, 2.296 Å and 1.68 Å. It is clear that the lattice constant decreased due to the

shorter bonding length and due an increase in the degree of ordering [16]. In addition the oxidation of the surface due to air annealing may account for the decrease in the unit cell parameters [17], [18]. This belief is confirmed by the EDS spectra for the annealed samples which are displayed in Fig. 2. The spectra of the annealed samples displayed much larger oxygen content (inset-1 of Fig. 2) compared to the as grown films. The oxygen contents in the samples increased by 13.67 at. %. Actually the ionic radius of oxygen being 1.35 Å [19] is larger than that of La (1.16 Å [20]) and larger than that of Ag (1.28 Å [21]). The direct substitution of oxygen in the $Ag_2La$ lattice is not expected. However the samples contained excess Ag which means some of the Ag was not completely bonded. As the average bond length of Ag-O is 2.127 Å [22] which is smaller than that of Ag1-Ag2 calculated here, Ag atoms on the surface would prefer reaching stability through formation of $Ag_2O$ on the surface of the film. It should be noted that silver oxide displayed diffraction patterns centered at $2\theta = 26.9^o$, $32.69^o$, $37.94^o$, $54.9^o$, $65.54^o$ and $69^o$ [23]. None of these peaks appeared in the XRD patterns (Fig. 1 (a)). Annealed $Ag_2La$ films display diffraction patterns at $2\theta = 16.10^o$, $25.80^o$, $28.6^o$, $38.40^o$, $40.20^o$, $44.20^o$ and $49.30^o$. Although the XRD technique did not explore this thin oxide layer, the scanning electron microscopy shown as inset-2 in Fig.2 indicates the formation of very dense layer of grains. The grains are hardly visible. An enlargement by 60000 times revealed the illustrated grains. The average grain size for the annealed samples is 80 nm. Grains of such sizes were not observed in the as grown films. In addition, the structural parameters for the annealed films are listed in Table-1. It is readable from table-1 that the crystallite sizes (accumulates to form a grain) become larger and the other parameters like strain, stacking faults and defect density decreased after the samples were annealed. Diffusion of oxygen at the grain boundaries could account for the increased crystallite sizes [24]. Completed bonding between excess Ag and excess oxygen could also accounts for the enhanced crystallinity of the $Ag_2La$ films [25].

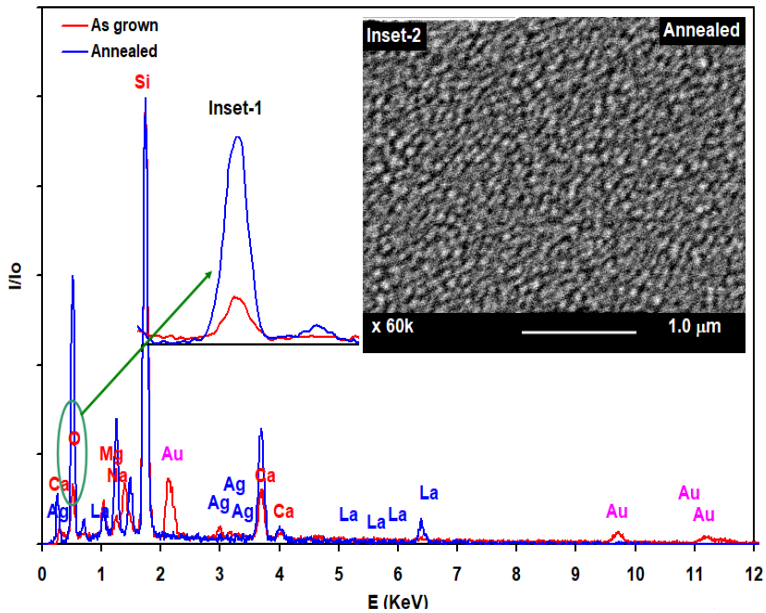


*Fig. 2. EDS spectra for as grown and annealed $Ag_2La$ thin films. The inset displaying the SEM images for the annealed films. Inset-1 showing the increase in oxygen content and inset-2 illustrating the SEM images for the annealed samples.*

Fig. 3 (a) illustrates the Arrhenius plot for the temperature dependent conductivities ($\sigma$) for the as deposited and heat treated $Ag_2La$ films. The room temperature electrical conductivity values are $6.05\times 10^{-6}\ (\Omega cm)^{-1}$ and $2.40\times 10^{-6}\ (\Omega cm)^{-1}$, respectively. The values of the electrical conductivities are very low indicating semiconductor or even insulator film characteristics. The electrical conductivity values are close to those of Ag based materials like

$AgGaS_2$, $AgGaSe_2$ [26]. As readable in the figure $\sigma(T)$ of the as deposited and annealed films is not varying with temperature in the temperature range of 300-340 K and 300-360 K, respectively. In the higher temperature range the $\sigma(T)$increases with increasing temperature showing different slopes of variations. The conductivity activation energy ($E_\sigma$) is calculated assuming the domination of current conduction by thermionic emission of charge carriers over the potential barriers formed by grain boundaries [27]. In accordance with the equation [27],

$$\sigma = \sigma_o \exp(-E_\sigma/kT), \tag{1}$$

one reveals $E_\sigma$ values of 252 meV and 180 meV in the temperature ranges of 340-440 K and 360-440 K for the as grown and annealed films, respectively. $\sigma_o$ in Eqn. (1) is the pre-exponential factor. Because $Ag_2La$ films are n-type, the conductivity activation energy should correspond to a donor level centered below the minima of the conduction band of $Ag_2La$. However, executing the derivative of the activation energy [27], and plotting it as function of temperature (inset of Fig. 3 (a)) one observe temperature dependent activation energy values. Such property means that the current conduction by thermionic emission are impure and there exist another possible current conduction mechanisms [28].

$$dE_\sigma(T) = -\frac{d(\ln(\sigma) - \ln(\sigma_o))}{d(kT^{-1})} \tag{2}$$

The electrical conductivity data is plotted assuming current conduction by variable range hopping (VRH) mechanism as a sharing mechanism to that of thermionic. In this mechanism the conductivity takes the form

$$\sigma = \sigma_1 e^{-\left(\frac{T_o}{T}\right)^{1/4}} \tag{3}$$

Here $\boldsymbol{T_o}$ is the degree of disorder and $\boldsymbol{\sigma_1}$ is a constant representing the pre-exponent value. This transport mechanism is preferable when the localized levels near Fermi level ($\boldsymbol{E_F}$) becomes continuously distributed. The hopping is actualized within an average hopping range and hoping energy given by the equations, respectively.

$$R = \left(\frac{9}{8\ \pi\ \gamma\ k_B\ T\ N(E_F)}\right)^{1/4} \tag{4}$$

and

$$W = \frac{3}{4\ \pi\ R^3\ N(E_F)} \tag{5}$$

In the above equations $\boldsymbol{N(E_F)}$ is the density of localized states near Fermi level and is determined from the relation,

$$T_o = \frac{18.1\gamma^3}{k_B N(E_F)} \tag{6}$$

Here $\boldsymbol{\gamma = \xi^{-1}}$. $\boldsymbol{\xi}$ is localization length (known as the decay constant). The current conduction by hopping mechanism are accepted to be valid mechanism if $\boldsymbol{W > kT}$, $\boldsymbol{T_o > 10^3\ K}$ and $\boldsymbol{\gamma R \gg 1}$.

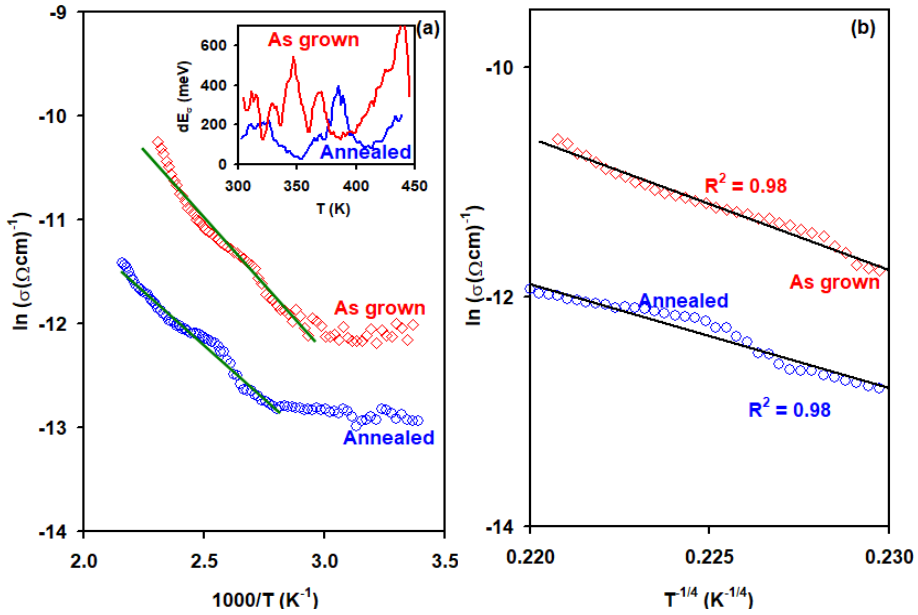


*Fig. 3. (a) the $\ln(\sigma) - T^{-1}$ and (b) the $\ln(\sigma) - T^{-1/4}$ plots for as grown and annealed $Ag_2La$ films. The inset of (a) demonstrating the conductivity activation energy as function of temperature.*

In the temperature range of 360-425 K, The linear fittings of the $\ln(\sigma)$-$T^{-1/4}$ variations which are shown in Fig. 3 (b) revealed slopes that allow determining the values of $T_o$. Other hopping parameters are then calculated with the help of Eqn. (4)- (6). These parameters are listed in Table-2. It is evident from the data that that the hopping conduction is highly preferable in these samples. The parameters are consistent with those reported for materials exhibiting current conduction by variable range hopping [27], [29], [30]. However we should recall here that the current conduction by VRH are an assisting conduction mechanism because at these high temperatures the thermionic emission is usually dominant mechanism [28].

It is also observed from the conductivity data analyses that the annealing of $Ag_2La$ samples decreased the electrical conductivity in all the studied temperature range. The most probable reason for the decreased conductivity values is the decrease in the free carrier concentration originating from excess Ag (in the as grown samples) which reacted with oxygen after annealing as confirmed from the EDS spectra shown in Fig. 2. Formation of $Ag_2O$ layer may behave as traps which limits free charge motions leading to the observed decrease in electrical conductivity [31]. In addition the conductivity activation energy also decreased from 252 meV to 180 meV. These energy values are close to the average hopping energy values (especially for the annealed samples) presented in Table-2 which also decreased upon annealing. The value of the conductivity activation energy being 180 meV is always observed in Ag based materials having $Ag_2O$ enriched in its structure [32]. Hence the shift in the activation energy is ascribed to the formation of $Ag_2O$ in the $Ag_2La$ films. It can be seen from the figure that the annealing process decreased the degree of disorder and decreased the average hopping distance. The degree of disorder decreases due to the decrease in defect density [33]. As seen from Table-1, the annealing process decreased the defect density from $3.99\times 10^{11}$ lines/cm$^2$ to $2.91\times 10^{11}$ lines/cm$^2$.

On the other hand the annealing of the $Ag_2La$ samples increased the density of localized states near Fermi level by more than 91.4%. The main factor affecting the density of states and their localizations are the position of Fermi level. Crossing of Fermi level with a trapping state created by impurities and/or defects may cause this increase. The annealing process decreased the defect concentration and caused capture of oxygen. Oxygen increases the hole concentration in the samples leading to a further localization [34], [35].

*Table 2. The VRH constants for the as grown and annealed $Ag_2La$ thin films.*

| Sample | slope | $\xi$(Å) | $\gamma$ ($10^7$ $cm^{-1}$) | $T_0$ ($10^7$ K) | $N(E_F)$ ($10^{18}$ $cm^3/eV$) | R(A) | W (meV) | $\gamma R$ |
|---|---|---|---|---|---|---|---|---|
| As grown | 106.3 | 10 | 1 | 12.80 | 1.64 | 89.16 | 206 | 8.92 |
| annealed | 90.4 | 10 | 1 | 6.68 | 3.14 | 75.82 | 175 | 7.58 |

It's noteworthy to emphasize that the fittings represented by the solid green line in Figures 3 (a) and (b) were conducted using a specialized high-convergence minimization algorithm, employing regression analysis and statistical tools such as residual sums of squares (R2), coefficient of determination, and residual mean squares. The data errors were assessed to range from 5% to 10%. Additionally, the calculated slope was constrained to ensure a residual sum of squares greater than 0.98.

## 4. Conclusions

In the current work we have shown the possible formation of $Ag_2La$ alloys from two stacked nanosheets of La and Ag. The films exhibited orthorhombic structure of lattice parameters of $a = 6.670$ Å$, b = 10.386$ Å$, c = 7.749$ Å. The material is formed due the preferred bonding mechanism between La and Ag. The structural and morphological analyses of the samples revealed an excess of silver in their composition compared to the desired stoichiometry. The crystallites sizes and grains exhibited average values of 29 nm and 400 nm, respectively. Electrical measurements have shown that the films shows electrical conductivity like those of poor semiconductors or insulators. The electrical conduction is dominated by a mixed current conduction mechanism composed of thermionic emission with an activation energy of 252 meV and by the variable range hopping conduction. On the other hand annealing the samples at 200 $^oC$ for one hour in air atmosphere increased the crystallite sizes and decreased the defect concentration as well as the microstrain and stacking faults percentages. The annealing increased the content of oxygen in the samples and shifted the conductivity activation energy to 180 meV. All the variable range hopping parameters are engineered accordingly. Exploring the structural and electrical properties of the $Ag_2La$ compound in thin film form will open the doors toward using these classes of material in low dimensional applications that require high resistive substrates.

### Acknowledgements

This work was supported by the Arab American University, Palestine and by Istinye University, Istanbul, Turkey. Therefore, the authors thank the Universities for its technical and financial support.

## References

[1] Bouala, GI Nkou, A. Etiemble, S. Dassonneville, C. Der Loughian, C. Langlois, J-F. Pierson, Philippe Steyer. Journal of Alloys and Compounds 851 (2021): 156908; https://doi.org/10.1016/j.jallcom.2020.156908

[2] Mishra, Surabhi, Pravin Kumar Singh, Rajesh K. Yadav, Ahmad Umar, Pooja Lohia, D. K. Dwivedi, Chemical Physics 541 (2021): 111021; https://doi.org/10.1016/j.chemphys.2020.111021

[3] Shpetnyi, Ihor Oleksandrovych, Kostiantyn Volodymyrovych Tyshchenko, Vasyl Yakovych Pak, B. V. Duzhyi, Yurii Oleksiiovych Shkurdoda, Ivan Yukhymovych Protsenko. Structural-Phase State and Magnetotransport Properties of Thin Film Alloys Based on Permalloy and Copper, (2021).

[4] Wei, Chenhuinan, ChenXia Kang, Qiming Liu, Nanotechnology 31, no. 11 (2019): 115501; https://doi.org/10.1088/1361-6528/ab59ea

[5] Watanabe, Tomofumi, Masafumi Takesue, Tomoki Matsuda, Tomokazu Sano, Akio Hirose, Journal of Materials Science: Materials in Electronics 31 (2020): 17173-17182; https://doi.org/10.1007/s10854-020-04265-y

[6] Mohanta, Maheswari, S. K. Parida, Ananya Sahoo, Mukul Gupta, V. R. R. Medicherla, Phase Transitions 94, no. 6-8 (2021): 445-453; https://doi.org/10.1080/01411594.2021.1944627

[7] Alfhaid, Latifah Hamad Khalid, Atef Fayez Qasrawi, Journal of Electronic Materials 52, no. 9 (2023): 6216-6224; https://doi.org/10.1007/s11664-023-10554-z

[8] Gschneidner, K. A., F. W. Calderwood, Bulletin of Alloy Phase Diagrams 4, no. 4 (1983): 370-374; https://doi.org/10.1007/BF02868082

[9] Rai, Hritika, Neha Kondal, Materials Today: Proceedings 48 (2022): 1320-1324; https://doi.org/10.1016/j.matpr.2021.08.343

[10] Zhao, Yaoxiao, Wangqiang Shen, Weixing Chen, Xing Lu, Inorganics 11, no. 7 (2023): 277; https://doi.org/10.3390/inorganics11070277

[11] Das, Shayeri, Prabhat Ranjan, Tanmoy Chakraborty, Nanotechnology-Enhanced Solid Materials, pp. 99-116. Apple Academic Press, 2023; https://doi.org/10.1201/9781003333449-5

[12] Zhang, Shuoxin, Shi-Yu Liu, Dali Yan, Qian Yu, Haitao Ren, Bin Yu, Dejun Li, Materials Chemistry and Physics 309 (2023): 128363; https://doi.org/10.1016/j.matchemphys.2023.128363

[13] Almotiri, R. A., A. F. Qasrawi, Physica Scripta 98, no. 4 (2023): 045806; https://doi.org/10.1088/1402-4896/acbb3a

[14] Wei, Lin, GuiLi Liu, JiaXin Wang, Guo Ying Zhang Materials Science and Engineering: B 297 (2023): 116785; https://doi.org/10.1016/j.mseb.2023.116785

[15] Sagadevan, Suresh, Solhe F. Alshahateet, J. Anita Lett, Is Fatimah, Ramesh Poonchi Sivasankaran, Assefu Kassegn Sibhatu, Estelle Leonard, Minh-Vien Le, Tetsuo Soga, Inorganic Chemistry Communications 148 (2023): 110288; https://doi.org/10.1016/j.inoche.2022.110288

[16] Kim, Taewoo, Eunpyo Hong, Youngkue Choi, Myunghyun Kim, Heesoo Lee, Advances in Applied Ceramics 117, no. 7 (2018): 414-419; https://doi.org/10.1080/17436753.2018.1472922

[17] Jia, Yanli, Ge He, Wei Hu, Hua Yang, Zhenzhong Yang, Heshan Yu, Qinghua Zhang et al., Scientific Reports 8, no. 1 (2018): 3995; https://doi.org/10.1038/s41598-018-22393-8

[18] Niwa, Koichi, Materials Science Monographs, vol. 81, pp. 341-351. Elsevier, 1995; https://doi.org/10.1016/S0166-6010(06)80012-3

[19] To, Theany, Alexandra AKRK Olsen, Bodil A. Hansen, Katrine M. Enevoldsen, Victor Lütken, Lars R. Jensen, Randall E. Youngman, Morten M. Smedskjaer, Journal of Non-Crystalline Solids 618 (2023): 122506; https://doi.org/10.1016/j.jnoncrysol.2023.122506

[20] Alfhaid, Latifah Hamad Khalid, Atef Fayez Qasrawi, Journal of Electronic Materials 52, no. 9 (2023): 6216-6224; https://doi.org/10.1007/s11664-023-10554-z

[21] Alharbi, Seham R., Atef F. Qasrawi, Sabah E. Algarni, Physica Status Solidi B 258, no. 5 (2021): 2000578; https://doi.org/10.1002/pssb.202000578

[22] Chen, Lanli, Xiaofang Wang, Siqi Shi, Yuanyuan Cui, Hongjie Luo, Yanfeng Gao. Applied Surface Science 367 (2016): 507-517; https://doi.org/10.1016/j.apsusc.2016.01.223

[23] Rajabi, Armin, Mariyam Jameelah Ghazali, Ebrahim Mahmoudi, Amir Hossein Baghdadi, Abdul Wahab Mohammad, Nadia Mohd Mustafah, Htwe Ohnmar, Amaramalar Selvi Naicker. Nanomaterials 9, no. 3 (2019): 450; https://doi.org/10.3390/nano9030450

[24] Suryavanshi, Priya S., Hardik Khunt, Bharati Rehani, C. J. Panchal, Materials Today: Proceedings 4, no. 14 (2017): 12500-12504; https://doi.org/10.1016/j.matpr.2017.10.051

[25] Qasrawi, Atef Fayez, Arwa N. Abu Ghannam, Optical and Quantum Electronics 54, no. 1 (2022): 4; https://doi.org/10.1007/s11082-021-03375-z

[26] Madelung, Otfried. Semiconductors: data handbook. Springer Science & Business Media, 2004; https://doi.org/10.1007/978-3-642-18865-7

[27] Qasrawi, Atef Fayez, Maryam Khalefa N. Abuarra, Applied Physics A 129, no. 9 (2023):

664; https://doi.org/10.1007/s00339-023-06955-w

[28] Ziqan, Abdelhalim M., A. F. Qasrawi, Abdulftah H. Mohammad, N. M. Gasanly. Bulletin of Materials Science 38 (2015): 593-598; https://doi.org/10.1007/s12034-015-0869-0

[29] Zhang, X. Y., J. S. Chawla, B. M. Howe, D. Gall, Physical Review B 83, no. 16 (2011): 165205; https://doi.org/10.1103/PhysRevB.83.165205

[30] Deshpande, S. K., S. N. Achary, Rohini Mani, J. Gopalakrishnan, A. K. Tyagi. Physical Review B 84, no. 6 (2011): 064301; https://doi.org/10.1103/PhysRevB.84.064301

[31] Heo, Young-Woo, S. J. Pearton, D. P. Norton, Journal of Nanoscience and Nanotechnology 12, no. 4 (2012): 3264-3267; https://doi.org/10.1166/jnn.2012.5635

[32] Kumar, E. Ramesh, K. Rajanikumari, B. Appa Rao, G. Bhikshamaiah, Int J Innovative Res in Sci, Eng and Tech 3, no. 4 (2014): 11271-11277.

[33] Boateng, Emmanuel, Jesse Smiles Dondapati, Antony Raj Thiruppathi, Aicheng Chen, International Journal of Hydrogen Energy 45, no. 53 (2020): 28951-28963; https://doi.org/10.1016/j.ijhydene.2020.07.128

[34] Qasrawi, A. F., Abdelhalim M. Ziqan, Suha Kh Jazzar, N. M. Gasanly, Physica B: Condensed Matter 458 (2015): 149-154; https://doi.org/10.1016/j.physb.2014.11.038

[35] Wang, Xuesong, Hongyuan Song, Chengchao Yang, Haorong Wu, Chen Zhang, Lan Yu, Journal of Materials Science: Materials in Electronics 34, no. 32 (2023): 2157; https://doi.org/10.1007/s10854-023-11559-4